Fischer, Andreas

Model-based review of Doppler global velocimetry techniques with laser frequency modulation

Journal Article as: peer-reviewed accepted version (Postprint)

DOI of this document*(secondary publication): https://doi.org/10.26092/elib/3301

Publication date of this document: 13/09/2024

* for better findability or for reliable citation

Recommended Citation (primary publication/Version of Record) incl. DOI:

Andreas Fischer, Model-based review of Doppler global velocimetry techniques with laser frequency modulation, Optics and Lasers in Engineering, Volume 93, 2017, Pages 19-35, ISSN 0143-8166, https://doi.org/10.1016/j.optlaseng.2017.01.004.

Model-based review of Doppler global velocimetry techniques with laser frequency modulation

Andreas Fischer

University of Bremen, Bremen Institute for Metrology, Automation and Quality Science (BIMAQ), Linzer Str. 13, 28359 Bremen, Germany

A R T I C L E I N F O

Keywords:
Doppler global velocimetry
Flow velocity measurement
Scattered light intensity fluctuations
Measurement uncertainty

A B S T R A C T

Optical measurements of flow velocity fields are of crucial importance to understand the behavior of complex flow. One flow field measurement technique is Doppler global velocimetry (DGV). A large variety of different DGV approaches exist, e.g., applying different kinds of laser frequency modulation. In order to investigate the measurement capabilities especially of the newer DGV approaches with laser frequency modulation, a model-based review of all DGV measurement principles is performed. The DGV principles can be categorized by the respective number of required time steps. The systematic review of all DGV principle reveals drawbacks and benefits of the different measurement approaches with respect to the temporal resolution, the spatial resolution and the measurement range. Furthermore, the Cramér-Rao bound for photon shot is calculated and discussed, which represents a fundamental limit of the achievable measurement uncertainty. As a result, all DGV techniques provide similar minimal uncertainty limits. With N_{photons} as the number of scattered photons, the minimal standard deviation of the flow velocity reads about $106\ \mathrm{m/s}/\sqrt{N_{\mathrm{photons}}}$, which was calculated for a perpendicular arrangement of the illumination and observation direction and a laser wavelength of 895 nm. As a further result, the signal processing efficiencies are determined with a Monte-Carlo simulation. Except for the newest correlation-based DGV method, the signal processing algorithms are already optimal or near the optimum. Finally, the different DGV approaches are compared regarding errors due to temporal variations of the scattered light intensity and the flow velocity. The influence of a linear variation of the scattered light intensity can be reduced by maximizing the number of time steps, because this means to acquire more information for the correction of this systematic effect. However, more time steps can result in a flow velocity measurement with a lower temporal resolution, when operating at the maximal frame rate of the camera. DGV without laser frequency modulation then provides the highest temporal resolutions and is not sensitive with respect to temporal variations but with respect to spatial variations of the scattered light intensity. In contrast to this, all DGV variants suffer from velocity variations during the measurement. In summary, the experimental conditions and the measurement task finally decide about the ideal choice from the reviewed DGV methods.

1. Introduction

The understanding of complex flow phenomena is a key to face the globally increasing needs for efficient and clean energy conversions, e.g., for the generation of electrical power as well as for transportation. Important aspects are the investigation of the fluid circulation around moving parts (aerodynamics) and respective losses (flow leakage, flow turbulence), the combustion of fuel (turbulent reactive flows), the generation and damping of noise (aeroacoustics) as well as sound-combustion interactions (thermoacoustics). However, the direct numerical simulation of turbulent flows is limited by the available computing power, whereas other numerical approaches require turbulence models. For this reason, measurements are inevitable either to directly investigate complex flows or to validate flow simulations and to improve them by identifying new phenomena.

One crucial physical quantity to be measured is the flow velocity. Non-intrusive, optical measurement principles that are based on Mie scattering at tracer particles can be divided into time-of-flight and Doppler principles:

- Time-of-flight principles evaluate the position $\vec{x}$ of tracer particles at given time steps, or vice versa, and then directly apply the velocity definition $\vec{v} = \frac{\partial \vec{x}}{\partial t}$. Examples for space-measurement-based time-of-flight principles are *Particle Tracking Velocimetry* [1–5] and *Particle Image Velocimetry* [1,6–10], and examples for time-measurement-based time-of-flight principles are *Laser-2-Focus Anemometry* [11–13] and *Spatial Filter Velocimetry* [14–16].
- The Doppler principles measure the frequency shift of the narrow-

E-mail address: andreas.fischer@bimaq.de.

band laser light scattered on tracer particles (usually Mie scattering) or fluid molecules (Rayleigh scattering). Then the flow velocity component, which is directly proportional to the Doppler frequency f_D and is the component along the bisecting line of the observation direction $\vec{o}$ and the negative laser incidence direction $-\vec{i}$, is calculated using the Doppler formula

$$v = \frac{\lambda}{|\vec{o} - \vec{i}|} f_D \tag{1}$$

with λ as laser wavelength. Note that $v = \frac{\vec{o} - \vec{i}}{|\vec{o} - \vec{i}|}\vec{v}$. Three different pairs of light incidence and observation directions are required to yield all three velocity components. For Mie scattering, which obviously allows to achieve higher light powers and therefore lower measurement uncertainties, the Doppler techniques can be subdivided into methods based on frequency and amplitude evaluation. Frequency evaluation means reducing the carrier frequency of the scattered light signal by light mixing and measuring the beat frequency with a photo detection unit. Examples for mixing with laser light that has no Doppler shift (reference methods) are *Reference Laser Doppler Anemometry* [17,18] and *Heterodyne Doppler Global Velocimetry* [19–21], and examples for mixing with laser light that has a (different) Doppler shift (difference methods) are *Laser Doppler Anemometry/Velocimetry* [22,23,18], the *Laser Doppler Velocity Profile Sensor* [24–26] and *Imaging Laser Doppler Velocimetry* [21]. Doppler principles with amplitude evaluation use transmission curves of optical filters for converting the changes in optical frequency to intensity changes, which finally can be detected with a photo detection unit (camera or single point detector). Examples for applying interferometric filters are *Michelson Spectrometer Laser Doppler Velocimeter* [27], *Doppler Picture Velocimetry* [28,29], *Michelson Interferometer Planar Doppler Velocimetry* [30,31], *Mach-Zehnder Interferometer Planar Doppler Velocimetry* [32,33] and *Fabry-Pérot Interferometer Planar Doppler Velocimetry* [34–37], whereas *Doppler Global Velocity (DGV)* (synonym *Planar Doppler Velocimetry (PDV)*) [38–44] uses atomic/molecular filters.

The article focuses on the progress of the DGV/PDV variants by conducting a model-based comparison of the measurement error with respect to three important and yet only partially considered error sources: photon shot noise, temporal fluctuations of the scattered light intensity, and temporal fluctuations of the flow velocity.

1.1. State-of-the-art

One key challenge for the DGV approaches is their inherent cross-sensitivity with respect to the intensity of the scattered light intensity, i.e., the detector output signal is sensitive to both the Doppler frequency and the light intensity. For this reason, at least two independent measurements are necessary.

The original DGV setup is based on a laser *without laser frequency modulation* [40]. Here a beam splitter is applied to the scattered light and the scattered light intensity is additionally, directly measured using a second camera, cf. Fig. 1a. Thereby only a single time step (camera frame) is required for obtaining a flow velocity field measurement. However, the original DGV setup requires two cameras. This might be problematic when no second camera is available or the correction of pixel misalignment errors by image dewarping techniques fails [45]. For this reason, single camera DGV approaches were developed. One approach (space multiplex) is to image both images onto a single camera, which reduces the pixel resolution of the flow measurement, cf. Fig. 1b [46].

Another approach (wavelength multiplex) is to use a color camera and to apply an additional laser with a different wavelength that is not affected by the optical filter [47,48]. However, the scattered light intensity of both lasers is not easily related to each other, because the scattered light intensity is, amongst others, influenced by the laser wavelength and the size (and shape) of the scattering particle, and the particle size is usually not constant. Thus, not different laser wavelengths but different laser frequencies have to be applied. Since light portions with near frequencies that vary with the Doppler shift are difficult to separate, camera images at different laser frequencies are successively taken (time multiplex).

This idea led to newer DGV approaches *with laser frequency modulation*, cf. Fig. 1c. They provide a single camera solution with full pixel resolution, but no single-shot measurement. For realizing the laser frequency modulation, a single modulated laser is usually applied avoiding additional lasers. Many principles of DGV systems with laser frequency modulation were developed: 2-ν-PDV [49,50], FSK-DGV (3-ν) [51,52], FSK-DGV (4-ν) [53], FM-DGV [54,55] and very recently CC-DGV [56,57]. The acronyms and principles are explained in detail in Section 2.

DGV techniques were applied for many different investigations ranging from high-speed (supersonic flows with several hundred meters per second) to low-speed flow phenomena (sound particle velocity with some millimeters per second) and concerning non-reactive/reactive, steady/unsteady flows, single phase/two-phase flows. Application fields are, e.g., the aerodynamics of cylinders, wings, jets and turbine blades [40,42–44,58,56], the aeroacoustics of liners [59–62], the thermoacoustics of combustors [63] as well the complex flow mechanics of boundary and gap flows [41,64–67], turbulent non-reactive flows (jets) [50,68], turbulent reactive flows (flames) [69,70] and two-phase flows (sprays) [71–75]. Although impressive measurements results have been achieved and detailed error analyses were performed for each of the new DGV principles with laser frequency modulation, a common treatment and a direct comparison of the different measurement approaches are missing. Thereby one fundamental concern, which has not yet been investigated thoroughly, has to be addressed in particular: the inherent cross-sensitivity of such DGV system with respect to temporal variations of the scattered light intensity. This cross-sensitivity is a direct consequence of the time multiplex approach, i.e., when using two or more subsequent images for the flow velocity measurement. Note further that this is in principle the same problem as for the wavelength multiplexing approach, although the underlying physics are different. Only for FM-DGV, first attempts to describe the resulting error are presented in [76], and an investigation of the influence of refractive index fluctuations that directly affect the scattered light intensity is described in [77]. However, a comparison of all DGV approaches regarding the measurement error that results from fluctuations of the scattered light intensity is missing. In addition, the behavior with respect to velocity fluctuations is unclear. Furthermore, a comparison of the minimum achievable measurement uncertainty is of interest.

1.2. Aim and outline of the article

The first aim of the article is to present a common model-based treatment of the DGV approaches with and without laser frequency modulation, which provides an overview and comparison of the different DGV measurement principles in Section 2. For all DGV approaches, the minimal achievable measurement uncertainty with respect to the photon shot noise is then investigated by evaluating the Cramér-Rao bound and comparing the different results in Section 3. Next, the error due to temporal fluctuations of the scattered light intensity is investigated for the different DGV approaches by employing a simulation. The numerical results and the respective comparison of the different DGV variants are presented in Section 4. The simulation is also applied for investigating the influence of velocity fluctuations on the measurement error. The resulting findings are explained in Section 5. Note that the article is focused on a model-based treatment. The used models have been successfully applied and validated in numerous experiments. The article closes with a summary and outlook.

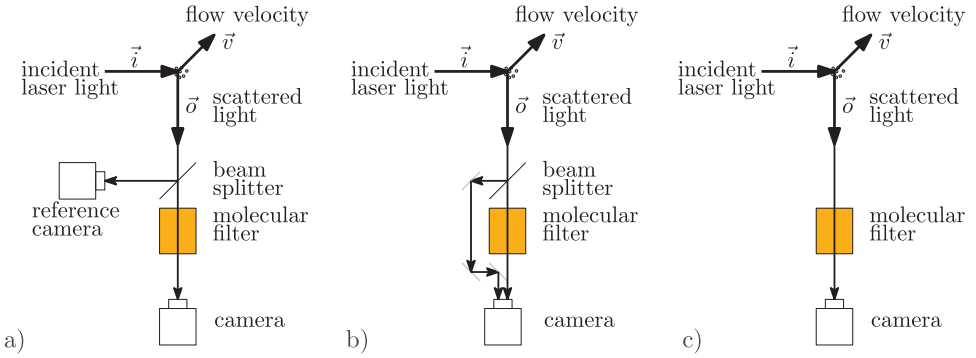

Fig. 1. Measurement arrangement of a) the original DGV approach with two cameras and the single-camera DGV approaches b) without and c) with laser frequency modulation. Note that the incident laser light is a light sheet that is imaged onto the cameras. The lenses of the imaging systems are not depicted here for the sake of clarity.

2. Common measurement principle and overview of the different approaches

The basis of all DGV approaches is a laser source, whose bandwidth is significantly smaller than the width of the transmission curve of the used molecular filter. The molecular filters are temperature-controlled absorption cells typically filled with iodine gas or cesium gas as absorber [78,79]. The gases provide several energy transitions (absorption lines) at the common laser wavelengths 514.5 nm, 532 nm, 852 nm, 895 nm. The corresponding transmission curves $\tau(f)$ over the light frequency f are shown in Fig. 2, which are calculated with validated models according to the literature references listed in Table 1.

For comparing the different DGV approaches, the transmission curve of the cesium D_1 line at 895 nm is arbitrarily chosen as the common transmission curve for the subsequent considerations. The full width at half maximum of this curve amounts to 600 MHz, and the absolute value of the derivative $\tau'(f)$ of the transmission function has two maxima at $\pm$ 300 MHz off the minimum transmission. The maxima offer the highest sensitivity with respect to a change in laser frequency (Doppler frequency). The proportionality factor between the flow velocity and the Doppler frequency here is 0.633 m/(s MHz) assuming a perpendicular arrangement of the laser illumination and the observation direction, cf. Eq. (1). Note that the flow velocity can always be converted into the corresponding Doppler frequency, and vice versa, by applying Eq. (1) for the given illumination and observation direction. Hence, presenting the subsequent findings either with respect to the flow velocity or the Doppler frequency is without loss of generality.

Note further that the different DGV variants do not depend on a certain molecular filter in principle. For this reason, only one (arbitrarily chosen) transmission curve is considered here as an example. However, each molecular filter has advantages and disadvantages. For instance, high-power lasers with the wavelengths 514.5 nm and 532 nm are available and the cameras have a high sensitivity for these

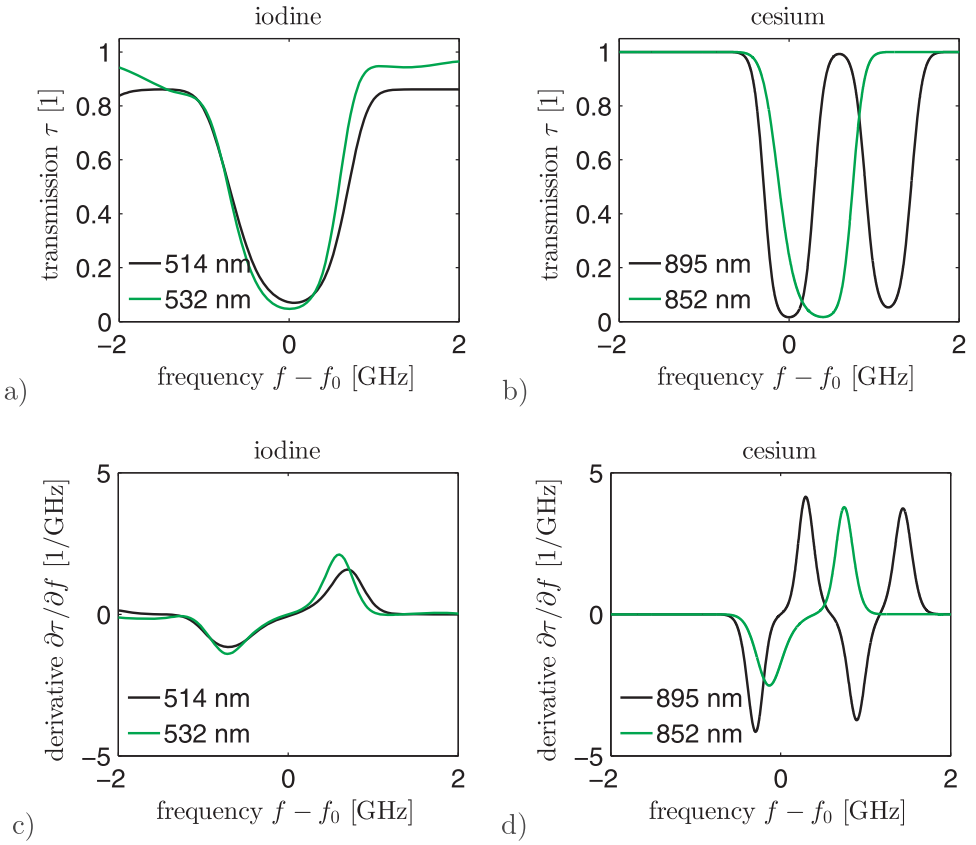

Fig. 2. Spectral transmission curves and their derivatives of cesium gas (a, c) and iodine gas (b, d), which are typically used for DGV. The respective offset light frequencies f_0, the references and the used parameters of the transmission models are listed in Table 1.

Table 1
Offset frequencies f_0, the corresponding vacuum wavelengths λ_0 and the literature references for the calculation of the transmission curves in Fig. 2 together with the model parameters cold finger temperature and body temperature of the 5 cm long absorption cells.

Gas	Frequency f_0	Wavelength λ_0	Ref.	Cold finger (°C)	Cell body (°C)
Cesium (D_1 line)	335.111370210561 THz	894.605449560 nm	[80,60]	35	45
Cesium (D_2 line)	351.721508283701 THz	852.357478685 nm	[80,81]	25	45
Iodine	582.491131261986 THz	514.673000000 nm	[82,50]	45	70
Iodine	563.263256648754 THz	532.242170000 nm	[82,83]	30	70

wavelengths. For this reason, molecular filters filled with iodine gas were initially used for DGV. On the other hand, continuous fast modulations of the laser frequency and high powers are obtained, e.g., with power amplified diode lasers with the wavelengths 852 nm and 895 nm. For this reason, molecular filters filled with cesium gas were initially chosen for DGV approaches that require a continuous fast modulation of the laser frequency. The currently available power of diode lasers, which can be used for cesium gas filters, is still lower in comparison with lasers for iodine gas filters. However, the sensitivity provided by the cesium transmission curve is higher than the sensitivity resulting from the iodine transmission curve, cf. Fig. 2c and d. Furthermore, molecular filters filled with rubidium gas were not yet used for realizing DGV systems, although their characteristics are similar to filters filled with cesium gas [79]. Finally, not only the laser power, the sensitivity of the molecular filter and the sensitivity of the camera, but also the scattering efficiency plays an important role for the resulting measurement uncertainty. Since this discussion about an optimal molecular filter is independent and out of the focus of the present article, only a single transmission curve is chosen for the desired comparison of the different DGV approaches.

With the scattered light intensity I_s, the light intensity I that is detected after the molecular filter reads

$$I = \tau(f)\cdot I_s. \tag{2}$$

Hence, one equation is available, but two unknown quantities exist: the Doppler shifted frequency f and the intensity I_s of the scattered light. In order to determine the Doppler shifted frequency, at least one further equation is required.

The different DGV approaches for the solution of this task are subsequently explained, where the approaches are categorized by the respective number N of the required time steps. The number of time steps equals the number of different laser frequencies. This categorization allows to classify all kinds of DGV principles. For every DGV principle, the light frequency f can be divided into the light center frequency f_c (including the Doppler shift frequency f_D) and a zero-mean laser frequency modulation $f_{mod}(t)$:

$$f = f_c + f_{mod}(t). \tag{3}$$

Note that the Doppler shift contained in the frequency modulation is neglected, because typical modulation amplitudes are more than eight orders of magnitude smaller than the absolute laser frequency. Considering DGV without laser frequency modulation, $f_{mod}(t)$ is zero. Otherwise the laser modulation contains different frequency steps, which yields the number of required time steps. In the following, the discrete-time modulation signal is denoted by $f_{mod,n}$ with $n = 1, \ldots, N$ as step number. The duration of one modulation period is $T = N\cdot t_a$ with t_a as the duration of one time step.

Since the modulation is zero-mean, the Doppler frequency f_D is always obtained by evaluating the difference between the center frequency f_c of the scattered light with Doppler shift and the center frequency $f_{c,0}$ of the laser light without Doppler shift:

$$f_D = f_c - f_{c,0}. \tag{4}$$

For this reason, the light center frequency is measured before and after the scattering in an analogous manner. Often the laser center frequency is kept constant by a laser frequency control (which also incorporates a measurement of the laser center frequency) and only the measurement of the Doppler shifted center frequency of the scattered light is processed further. The latter condition is assumed here, and the remaining fluctuations of the laser center frequency are considered to be negligibly small compared to the measurement uncertainty of the Doppler-shifted center frequency f_c of the scattered light. Hence, the subsequent considerations can be reduced to the measurement of f_c.

For all DGV measurement principles, the input signal is the intensity of the scattered light that is Doppler shifted in frequency. The times series of the incoming light intensity signal with $N \geq 1$ time steps reads according to Eqs. (2) and (3)

$$I_n = \tau(f_c + f_{mod,n})\cdot I_s, \quad n = 1, \ldots, N. \tag{5}$$

Note that the scattered light intensity is initially assumed to be constant during one modulation period. DGV measurement principles without laser frequency modulation require at least one time step and DGV measurement principles with laser frequency modulation require more than one time step. The different DGV measurement principles all provide a certain output quantity denoted as quotient q, which is independent of the scattered light intensity and only depends on f_c. As a result, the calibrated relation q over f_c is the calibration curve, which (after inversion) allows to derive the measurement result of f_c out of the measured value of q. This general measurement schema is depicted in Fig. 3. The specific determination of the quantity q is subsequently described for each DGV approach followed by a concluding comparison.

2.1. One time step (1-ν-DGV)

The original DGV and its variant with a single camera are DGV principles without laser frequency modulation, i.e.,

$$f_{mod,1} = 0, \tag{6}$$

cf. Fig. 4a. Applying a beam splitter with the specific beam split ratio 50/50, the incoming light intensity signal is split and the two detected light intensities read

$$I_{1,1} = \frac{1}{2}\cdot\tau(f_c)\cdot I_s \tag{7a}$$

$$I_{1,2} = \frac{1}{2}\cdot I_s. \tag{7b}$$

By dividing both detected intensities the quotient

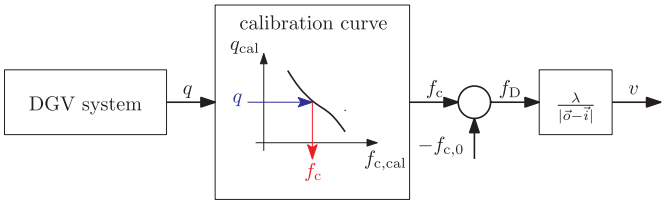

Fig. 3. General signal flow for all DGV systems providing an output quantity q as a function of the desired center frequency f_c of the scattered light, which finally yields the Doppler frequency f_D and the flow velocity v.

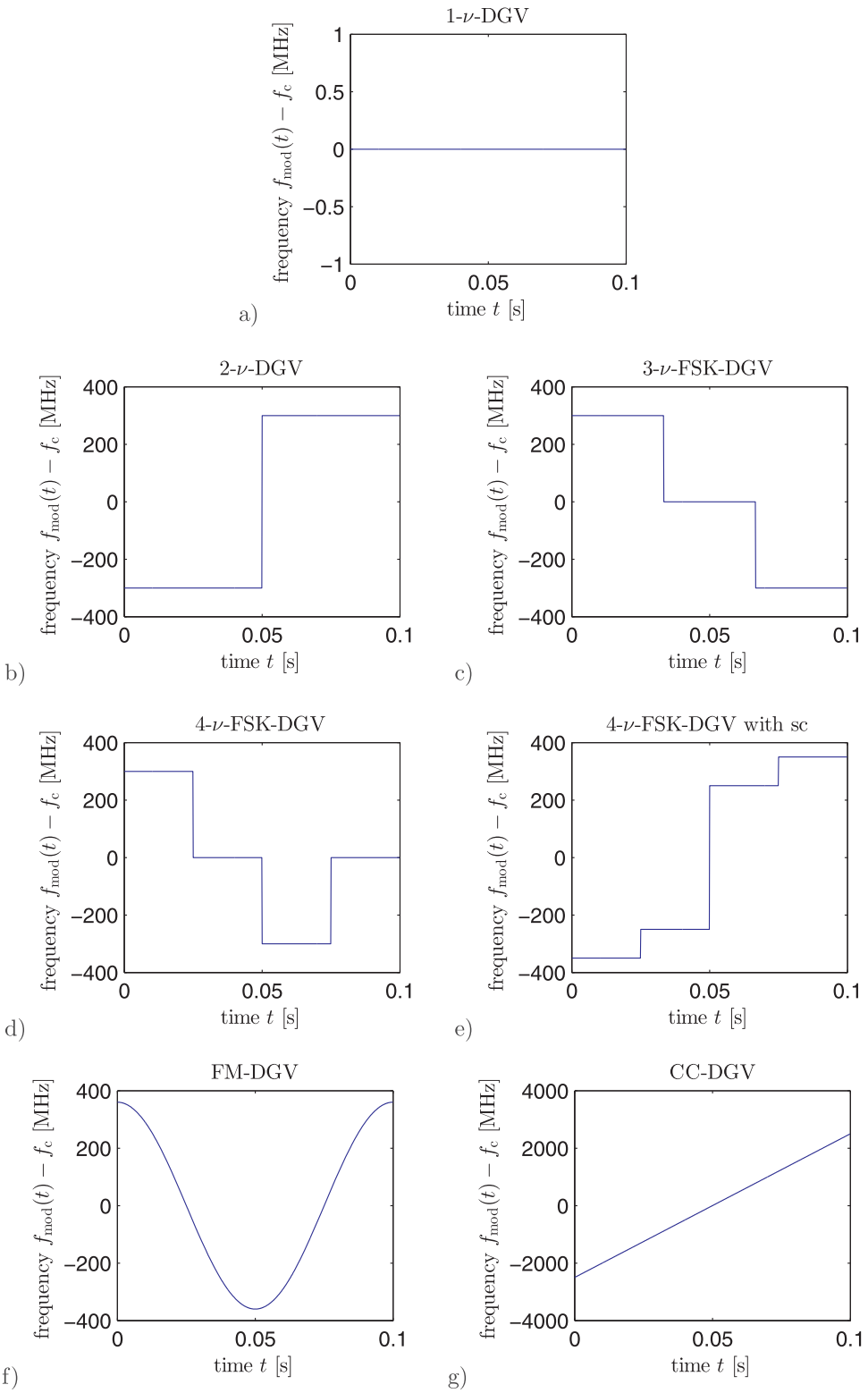

Fig. 4. Modulated laser frequency $f_{\mathrm{mod}}(t)$ minus the light center frequency f_{c} over one modulation period (here: $T = 0.1$ s) for the different DGV approaches.

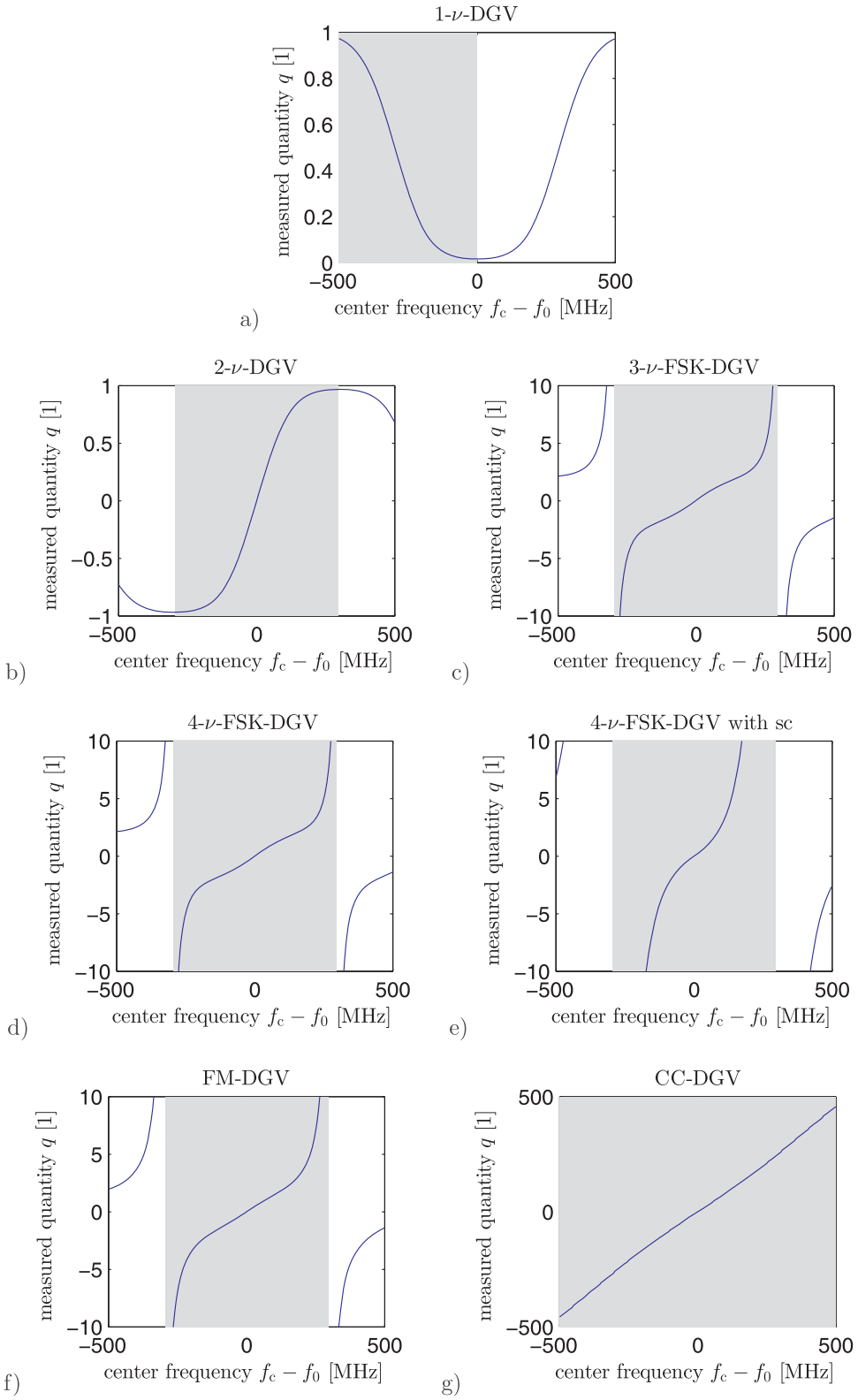

Fig. 5. Calibration curves of q over f_c for the different DGV approaches, when applying the laser frequency modulations shown in Fig. 4 and the transmission curve of cesium gas at f_0 = 335.111370210561 THz (cesium D_1 line), cf. Fig. 2 and Table 1. The gray region illustrates the measurement range, for which the calibration curve is unambiguous.

$$q = \frac{I_{1,1}}{I_{1,2}} = \tau(f_c) \tag{8}$$

is evaluated, which is independent of I_s. The dependency of the quotient q with respect to f_c is shown in Fig. 5a. Note that the two-color DGV approach can be described by the same set of equations and is therefore not treated separately.

2.2. Two time steps (2-ν-DGV)

For two-frequency DGV, one modulation period contains two frequencies and, thus, two time steps with

$$f_{\mathrm{mod},1} = -f_{\mathrm{h}} \tag{9a}$$

$$f_{\mathrm{mod},2} = +f_{\mathrm{h}}. \tag{9b}$$

The modulation with the amplitude $f_{\mathrm{h}} = 300$ MHz is depicted in Fig. 4b. Note that the modulation amplitude is chosen to operate with maximum sensitivity, i.e., the laser frequencies are located at the edges of the transmission curve where the absolute value of its derivative is maximal [50]. With the detected intensities I_1, I_2 according to Eq. (5), the quotient q is calculated by

$$q = -\frac{I_1 - I_2}{I_1 + I_2}. \tag{10}$$

Due to the division of intensities that are all directly proportional to the scattered light intensity, the latter is canceled. The quotient q is shown in Fig. 5b as a function of the light center frequency f_c.

The underlying idea of the quotient calculation resulted from the solution of a system of linear equations, where the intensity signals are linearized for $f_c \approx f_0$. The respective consideration was originally performed in time domain [50]. However, the calculation can also be interpreted in frequency domain, because the quotient is proportional to the ratio of the first Fourier coefficient (alternating component) and the mean value (direct component) of the intensity signal consisting of two samples. When using the direct component, the measurement has a cross-sensitivity with respect to the background light. In order to avoid this, a third equation is required.

2.3. Three time steps (3-ν-FSK-DGV)

When using three frequencies, the modulation reads

$$f_{\mathrm{mod},1} = +f_{\mathrm{h}} \tag{11a}$$

$$f_{\mathrm{mod},2} = 0 \tag{11b}$$

$$f_{\mathrm{mod},3} = -f_{\mathrm{h}}, \tag{11c}$$

cf. Fig. 4c for $f_{\mathrm{h}} = 300$ MHz. Using the detected intensities I_1, I_2, I_3 that follow from Eq. (5), the quotient

$$q = 2\frac{(I_1 - I_2) - (I_3 - I_2)}{(I_1 - I_2) + (I_3 - I_2)} = 2\frac{I_1 - I_3}{(I_1 - I_2) + (I_3 - I_2)} \tag{12}$$

is independent of the scattered light intensity and a constant background light intensity [52]. This approach is named frequency shift keying DGV (FSK-DGV). The resulting curve of the quotient q versus f_c is shown in Fig. 5c.

For $f_c \approx f_0$ the transmission of the scattered laser light is almost zero and, thus, I_2 serves as a measure of the background light intensity. As a result, the calculation of the quotient q here includes a subtraction of the background light intensity from the desired intensity measurements at the edges of the transmission curve, cf. Eq. (12) with Eq. (10). This explanation in time domain can also be understood in frequency domain, because the quotient q represents the ratio of the first to the second Fourier coefficient of the intensity signal [52]. Due to symmetry reasons, the fourth sample that is required for a Fourier analysis with two harmonics equals the second sample ($I_4 = I_2$) and, thus, the three samples are sufficient.

2.4. Four time steps (4-ν-FSK-DGV)

With four-frequency DGV, one option is to enhance the modulation to

$$f_{\mathrm{mod},1} = +f_{\mathrm{h}} \tag{13a}$$

$$f_{\mathrm{mod},2} = 0 \tag{13b}$$

$$f_{\mathrm{mod},3} = -f_{\mathrm{h}} \tag{13c}$$

$$f_{\mathrm{mod},4} = 0. \tag{13d}$$

Aside from the additional fourth sample, it is identical to the approach of 3-ν-FSK-DGV, but the quotient now is calculated out of all four detected intensities I_1, I_2, I_3 and I_4 by

$$q = 2\frac{(I_1 - I_2) - (I_3 - I_4)}{(I_1 - I_2) + (I_3 - I_4)}. \tag{14}$$

This enhanced approach is here termed 4-ν-FSK-DGV. The corresponding modulation and calibration curves are shown in Figs. 4d and 5d, respectively.

Using four instead of three frequency steps can provide an additional benefit for the measurement, which led to the development of a 4-ν-FSK-DGV with self-calibration (sc) [52]. For this purpose, the modulation is changed to

$$f_{\mathrm{mod},1} = -f_{\mathrm{h}} - f_{\mathrm{sh}} \tag{15a}$$

$$f_{\mathrm{mod},2} = -f_{\mathrm{h}} + f_{\mathrm{sh}} \tag{15b}$$

$$f_{\mathrm{mod},3} = +f_{\mathrm{h}} - f_{\mathrm{sh}} \tag{15c}$$

$$f_{\mathrm{mod},4} = +f_{\mathrm{h}} + f_{\mathrm{sh}}, \tag{15d}$$

see Fig. 4e. The employed modulation amplitude $f_{\mathrm{h}} = 300$ MHz and the additional shift frequency $f_{\mathrm{sh}} = 50$ MHz are set so that for $f_c \approx f_0$ two frequencies are located at the left edge and two frequencies are located at the right edge of the transmission curve. By evaluating the quotient

$$q = \frac{-I_1 - I_2 + I_3 + I_4}{I_1 - I_2 - I_3 + I_4} \tag{16}$$

the cross-sensitivity with respect to the slopes of the edges is eliminated, as long as the edges can be treated as linear functions [53]. The behavior of q versus f_c is shown in Fig. 5e.

2.5. More than four time steps (FM-DGV, CC-DGV)

Applying the FSK-DGV approach with signal evaluation in the frequency domain (Fourier analysis) towards a continuous sinusoidal laser frequency modulation with

$$f_{\mathrm{mod},n} = f_{\mathrm{h}} \cdot \cos\left(2\pi \frac{n-1}{N}\right), \quad n = 1, \ldots, N \tag{17}$$

leads to the concept of frequency modulation DGV (FM-DGV). The duration of one modulation period is $T = N \cdot t_{\mathrm{a}}$ with N as the the number of samples and t_{a} as the sampling period. For the modulation amplitude $f_{\mathrm{h}} = 300$ MHz, the modulation signal is shown in Fig. 4f. Evaluating the ratio of the first to the second Fourier coefficient of the intensity signal I_n (that is measured according to Eq. (5)), the quotient q results in [54]

$$q = \frac{\sum_{n=1}^{N} I_n \cdot \cos\left(\frac{2\pi}{T} \cdot t_{\mathrm{a}} \cdot (n-1)\right)}{\sum_{n=1}^{N} I_n \cdot \cos\left(\frac{4\pi}{T} \cdot t_{\mathrm{a}} \cdot (n-1)\right)}. \tag{18}$$

Note that the Fourier coefficients are determined using the phase reference that is given by the modulation signal. The resulting curve

Table 2
DGV approaches categorized by the required number of time steps with signal evaluation in time or frequency domain.

Required number of time steps	Name	Time domain	Frequency domain
1	1-ν-DGV	x	x
2	2-ν-DGV	x	x
3	3-ν-DGV	x	x
4	4-ν-FSK-DGV	x	x
	4-ν-FSK-DGV with sc	x	
>4	FM-DGV		x
	CC-DGV	x	

of q over f_c is shown in Fig. 5f. Using more than four time steps allows to reduce the influence of fluctuations of the scattered light, which occur as side-bands of the harmonics. In addition, sinusoidal laser frequency modulation can be realized faster than the necessary frequency steps for a discrete frequency modulation. For this reason, FM-DGV is advantageous for fast continuous measurements.

The most recent DGV development also uses more than four time steps, but uses a time domain evaluation. The idea is to capture a linear frequency scan of the entire transmission curve and to perform a cross-correlation between the detected intensity signal I_n and a reference transmission curve without Doppler shift [56,57]. The maximum of the cross-correlation then gives the output quantity q. This approach is named cross-correlation DGV (CC-DGV). The linear laser frequency modulation

$$f_{\mathrm{mod},n} = f_h \cdot \left(2 \cdot \frac{n-1}{N} - 1\right), \quad n = 1, \ldots, N \tag{19}$$

is shown in Fig. 4g with $f_h = 2500$ MHz to cover the entire transmission curve. The resulting intensity signal I_n is then cross-correlated with the transmission curve without Doppler shift for a range of lags from -5 to $+5$ sampling steps. This section of the cross-correlation is fitted by a parabolic function in order to determine the interpolated position q of the maximum. The so obtained quantity q as a function of f_c is shown in Fig. 5g. The fit results in systematic errors, which explains the non-linearity of the calibration curve. The known benefit of the correlation approach is the almost unlimited measurement range. Hence, CC-DGV is advantageous for flows with a large dynamic range of the flow velocity.

2.6. Comparison

The described DGV approaches are summarized in Table 2. They differ in the required number of time steps, which leads to different temporal resolutions when being limited by the maximum camera frame rate. The temporal resolution equals the period time of one modulation. Being limited by the camera frame rate, the 1-ν-DGV provides the highest temporal resolution. Note that for a limited memory space of the camera, the lowest number of frames per measurement also results in the largest possible number of successive measurements. The spatial resolution, which is determined by the camera pixel size and the magnification of the imaging system, is always the same. Except for the enhanced original DGV approach with a single camera, cf. Section 1.1, the field of view is also the same for all DGV measurement principles.

Each DGV technique provides an output quantity q, which depends on the center frequency f_c of the scattered light frequency as shown in Fig. 5. The unambiguous regions of these curves can be used to determine f_c out of the DGV output quantity q. The respective measurement ranges are illustrated by a gray background. For the 1-ν-DGV approach, the unambiguous region is one of the edges of the transmission curve, which covers a frequency range of about 500 MHz. For the 2-ν-DGV, 3-ν-FSK-DGV, 4-ν-FSK-DGV, 4-ν-FSK-DGV with self-calibration and FM-DGV, the measurement range equals about the region between the two extremal values of the derivative of the transmission curve, which amounts to 600 MHz. The CC-DGV approach provides a measurement range that is not limited by the properties of the transmission curve, but only by the width of the frequency scan. By adapting the scan width, the measurement range is in principle unlimited.

The measurement uncertainty of all DGV approaches is limited by random error sources such as thermal noise and shot noise of the photo detection unit. However, even if the photon detection is ideal (noise-free), the natural fluctuations of the detected light intensities due to photon shot noise are one fundamental limit for the achievable measurement uncertainty. In order to compare the ultimate measurement capabilities of the DGV principles, the Cramér-Rao bound for the photon shot noise is calculated for all DGV approaches and compared with each other in Section 3.

The DGV approaches were shown to have different cross-sensitivities, e.g., with respect to the background light. Such cross-sensitivities require a calibration in order to eliminate the systematic errors. One common source of systematic errors that cannot be corrected are variations of the scattered light intensity. While the original DGV approach with one time step is sensitive regarding spatial variations, the DGV approaches with more than one time step are all sensitive regarding temporal variations of the scattered light intensity. The error due to a temporal scattered light variation is investigated in Section 4.

Furthermore, note that all DGV measurement principles are derived for the condition of a constant flow velocity. For this reason, the error resulting from a temporal velocity variation is studied in Section 5.

3. Quantum noise limit

According to [84], the Cramér-Rao bound (CRB) of the flow velocity v with respect to the photon shot noise reads for DGV without laser frequency modulation (1-ν-DGV)

$$\mathrm{CRB}(v) = \frac{\lambda^2}{|\vec{o} - \vec{i}|^2} \cdot \frac{\tau(f_c) + \tau(f_c)^2}{\tau'(f_c)^2} \cdot \frac{2}{N_{\mathrm{photon}}} \tag{20}$$

and for DGV with laser frequency modulation (2-ν-DGV, 3-ν-FSK-DGV, 4-ν-FSK-DGV, 4-ν-FSK-DGV with sc, FM-DGV, CC-DGV)

$$\mathrm{CRB}(v) = \frac{\lambda^2}{|\vec{o} - \vec{i}|^2} \cdot \frac{\sum_{n=1}^{N} \tau_n}{\left(\sum_{n=1}^{N} \frac{\tau'^2_n}{\tau_n}\right) \cdot \left(\sum_{n=1}^{N} \tau_n\right) - \left(\sum_{n=1}^{N} \tau'_n\right)^2} \cdot \frac{N}{N_{\mathrm{photon}}} \tag{21}$$

with the abbreviations $\tau_n = \tau(f_c + f_{\mathrm{mod},n})$ and $\tau'_n = \tau'(f_c + f_{\mathrm{mod},n})$. The symbol N_{photon} is the total number of photons, which are scattered during one modulation period. One modulation period consists of N time steps. When measuring over $M \in \mathbb{N}$ modulation periods, the Cramér-Rao bound is reduces by the factor $1/M$. Here, only the case $M = 1$ is considered.

The square root of the calculated Cramér-Rao bounds for the different DGV approaches are shown in Fig. 6 over the light center frequency f_c as dashed lines. The applied parameters are the laser wavelength $\lambda = 895$ nm, the transmission curve $\tau(f)$ of cesium gas (cf. Fig. 2), the modulation period $T = 0.1$ s and a scattered light power of 1 nW, which corresponds to $N_{\mathrm{photon}} = 450553035$ photons, as well as a perpendicular arrangement of the illumination and observation direction ($\vec{o} \perp \vec{i}$, i.e., $|\vec{o} - \vec{i}| = \sqrt{2}$). The light center frequency f_c is varied over a range of 400 MHz within the measurement range. For the chosen laser wavelength and the measurement arrangement, this corresponds to a velocity range of 253 m/s, cf. Section 2.

As a result, the Cramér-Rao bounds of the different DGV approaches result in similar limits of the measurement uncertainty in the order of 0.01 m/s. In the strict sense, 2-ν-DGV provides the minimal uncertainty,

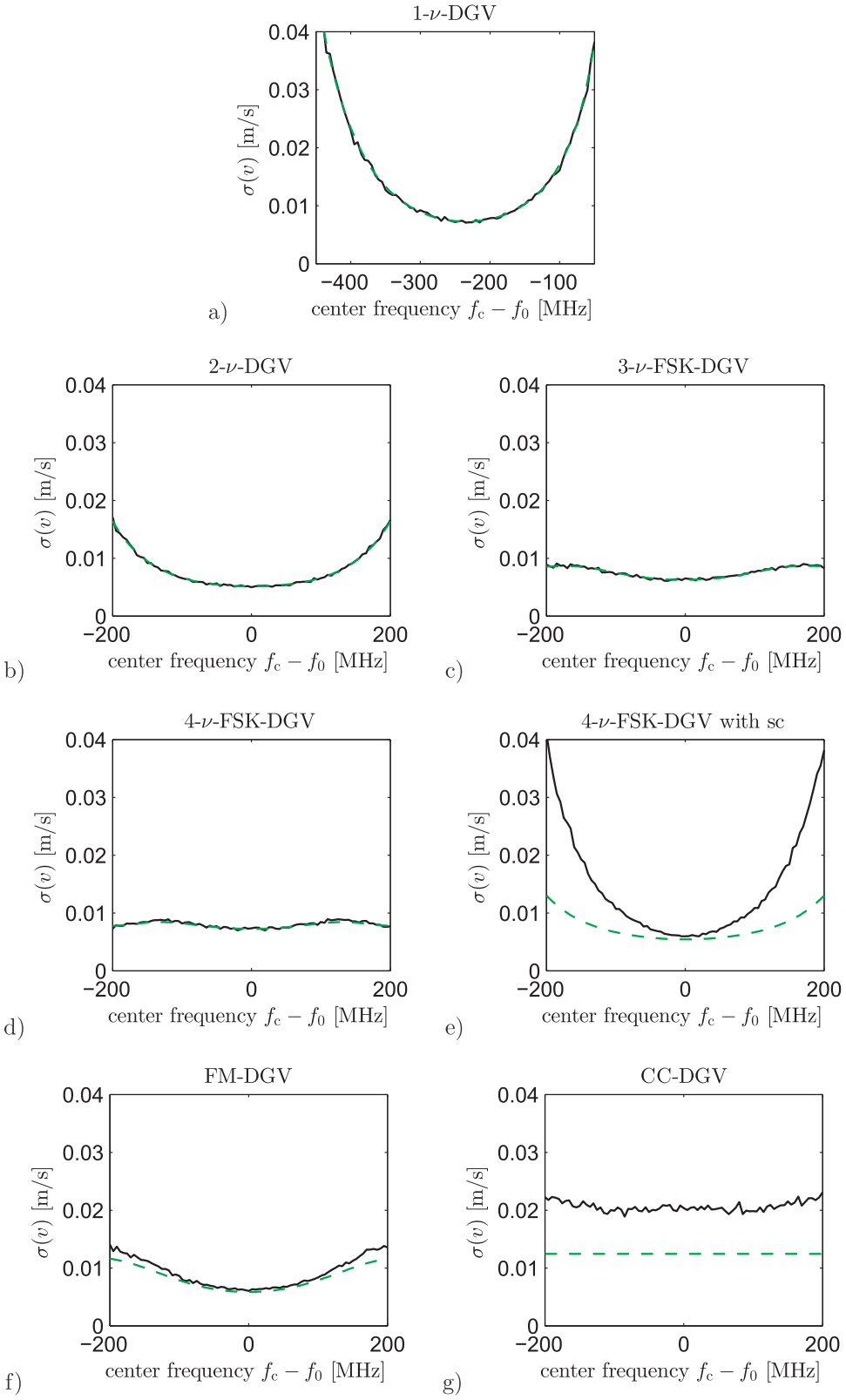

Fig. 6. Velocity standard deviation versus the light center frequency for the different DGV for photon shot noise (white Poissonian noise). The black solid lines are the results from a Monte-Carlo simulation with a sample size of 1000, and the green dashed lines are the square root of the calculated Cramér-Rao bound indicating the minimum achievable measurement uncertainty. The number of scattered photons is $N_{\text{photons}} = 450553035$, which equals a scattered light power of 1 nW for the modulation period $T = 0.1$ s and the laser wavelength $\lambda = 895$ nm. (For interpretation of the references to color in this figure legend, the reader is referred to the web version of this article.)

cf. the list in Table 3. The minimum is at $f_c \approx f_0$ and occurs due to the optimal use of the maximal system sensitivity without wasting information. For instance with 1-ν-DGV, 50% of the scattered light is only used in order to determine the scattered light intensity disregarding the contained frequency information. On the other hand, CC-DGV scans the entire transmission curve including locations with zero slope and, thus,

Table 3
Minimum square root of the Cramér-Rao bound and maximum square root of the estimation efficiency for each DGV approach, cf. Fig. 6.

DGV technique	$\min(\sqrt{\mathrm{CRB}(v)})$ (m/s)	$\max\left(\sqrt{\frac{\mathrm{CRB}(v)}{\mathrm{Var}(v)}}\right)$ (%)
1-ν-DGV	0.007	100
2-ν-DGV	0.005	100
3-ν-DGV	0.006	100
4-ν-FSK-DGV	0.007	100
4-ν-FSK-DGV with sc	0.005	91
FM-DGV	0.006	95
CC-DGV	0.012	62

zero sensitivity with respect to changed of the light center frequency. In other words, the time is partially 'wasted' by measurements with low sensitivity. This phenomenon is most significant for CC-DGV, whose minimal uncertainty is highest. For CC-DGV, the inverse of the Cramér-Rao bound, which is a measure of the information, and the adjustable measurement range fulfill an uncertainty relation, i.e., the higher measurement uncertainty is due to the higher measurement range. However, the effect of wasting information applies for all other DGV principles with laser frequency modulation. Within a range of 400 MHz, the Cramér-Rao bounds for all DGV approaches with laser frequency modulation yield a fundamental uncertainty limit between 0.005 m/s and 0.016 m/s. In contrast to this, the uncertainty limit of the original DGV approach without laser frequency modulation is strongly increasing at the outer regions of the evaluated frequency range. As a result, the measurement range seems to be limited most for the 1-ν-DGV. The reason is again the decreasing sensitivity when leaving the edge center of the transmission curve.

In order to evaluate the estimation efficiency of the employed signal processing algorithms (= ratio of the estimator variance to the Cramér-Rao bound), a Monte-Carlo simulation with a sample size of 1000 was performed using the software MATLAB for all DGV measurement principles. The simulation contains the signal evaluation of the intensity signals at the detector and is based on the descriptions in Section 2. The photon shot noise is implemented as white Poissonian noise. No systematic errors occurred for the chosen parameters. Hence, the calculated Cramér-Rao bound, which is only valid for unbiased estimators, can be applied. The resulting standard deviations of the simulated flow velocity measurements are shown in Fig. 6 as solid lines. For 1-ν-DGV, 2-ν-DGV, 3-ν-FSK-DGV and 4-ν-DGV, the standard deviations attain the uncertainty limits according to the Cramér-Rao bounds and, thus, offer an estimation efficiency near 100%. For FM-DGV, the standard deviation according to the Monte-Carlo simulation slightly diverges from the Cramér-Rao bound at the outer regions of the given frequency range, which is considered to be negligible. In contrast to this, the increasing loss of estimation efficiency towards the outer regions of the frequency is notable for the 4-ν-FSK-DGV with sc. It is assumed that the non-fulfillment of the underlying assumption of the signal processing algorithm, namely the non-linearity of the edges of the transmission curve, is responsible for this behavior. Considered CC-DGV, the standard deviation according to the Monte-Carlo simulation is about a factor of two larger than the limit from the Cramér-Rao bound. Hence, the evaluation of the cross-correlation function by employing a parabolic fit for eleven values appears to be sub-optimal and is assumed to allow future improvements. This conclusion can also be drawn when comparing the maximal efficiencies of the different DGV approaches, which are listed in Table 3. In general, however, the estimation efficiency of the signal processing algorithms can be considered as satisfactory for all DGV approaches, because the achievable standard deviations are not more than a factor of two to three larger than the uncertainty limit according to the Cramér-Rao bound.

Finally, the quantitative dependency of the fundamental uncertainty limit with respect to the number of scattered photons N_{photons} is demonstrated. For this purpose, the measurement condition that yields for $N_{\mathrm{photons}} = 450553035$ the minimal standard deviation 0.005 m/s is briefly considered as an example. Since the Cramér-Rao bound is indirectly proportional to N_{photons}, it then follows

$$\sqrt{\mathrm{CRB}(v)} = \frac{106.\ 13\ \mathrm{m/s}}{\sqrt{N_{\mathrm{photons}}}}. \tag{22}$$

This simple but fundamental relation, which applies for Poissonian photon shot noise, allows quick calculations of the ultimate limit of the DGV measurement uncertainty with respect to the available number of scattered photons.

It is mentioned for the sake of completeness that the importance of photon shot noise depends on the available scattered light intensity, the noise features of the detector and laser frequency stabilization. For low intensities, intensity independent noise sources such as the thermal noise, the dark current noise and the quantization noise from the photo detection dominate. For higher intensities, the electron shot noise of the photo detector dominates, which contains the photon shot noise, and an amplification excess noise might be important as well. Above a certain intensity level, the dominating noise source are the remaining random fluctuations of the stabilized laser center frequency [60]. As a result, photon shot noise is usually one of multiple contributions to the total measurement uncertainty, but it is always a fundamental natural lower limit of the measurement uncertainty.

4. Fluctuations of the scattered light power

A common concern regarding the newer DGV approaches with laser frequency modulation is their inherent cross-sensitivity with respect to temporal variations of the scattered light intensity. One typical reason for these fluctuations of the scattered light is the fluctuating number of scattering particles in the observed measurement volume, because the distribution of the scattering particles is random. The fluctuating concentration of the scattering particles in the flow can also lead to a non-constant attenuation of the incident or scattered light, which can cause fluctuations of the scattered light intensity. If speckles occur in the camera images due to the coherence of the laser light source, both described phenomena yield moving speckles also causing scattered light fluctuations.

In order to determine and discuss the errors due to scattered light fluctuations, a respective MATLAB simulation is performed for all DGV techniques. The noise is set to zero and the scattered light intensity I_{s}, which was introduced in Section 2 as a constant parameter, is now implemented with a linear increase over the measurement time $M{\cdot}T$, where T remains the duration of one modulation cycle consisting of N time steps and $M \in \mathbb{N}$ is the number of modulation cycles. For the mean value $\bar{I}_{\mathrm{s}}$ and the relative variation $I_{\mathrm{s},\Delta}$ of the scattered light intensity, the implemented discrete-time signal of the scattered light intensity reads

$$I_{\mathrm{s},i} = \bar{I}_{\mathrm{s}}{\cdot}\left(1 + I_{\mathrm{s},\Delta}{\cdot}\left(\frac{i}{N{\cdot}M} - \frac{1}{2}\right)\right),$$
$$i = 0,\ 1,\ \ldots,\ N{\cdot}M - 1. \tag{23}$$

The resulting deviation $\Delta(v)$ of the simulated measurement result from the true velocity value is calculated and compared for two important cases:

- The modulation period is equal (laser-limited condition).
- The modulation period is different (camera-limited condition).

However, the measurement time $M{\cdot}T$ is always the same, which allows a fair comparison. Here, the number of photons scattered during the measurement time is $M{\cdot}N_{\mathrm{photons}} = 450553035$, which agrees for $M = 1$ with the simulation condition in Section 3.

For the first case of equal modulation periods (laser-limited condi-

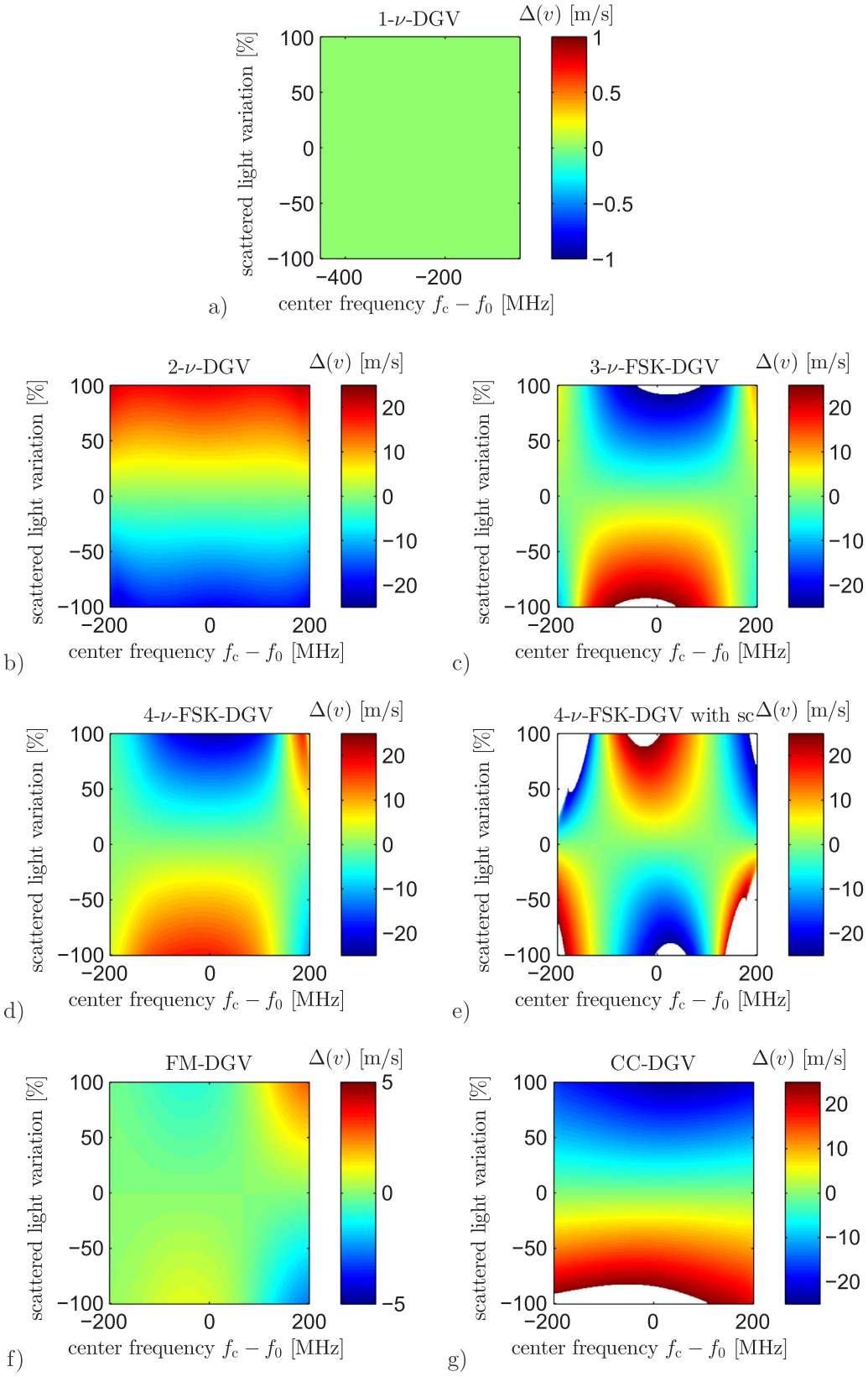

Fig. 7. Systematic velocity error for the different DGV approaches under *laser-limited condition* resulting from a linear variation of the scattered light power. The measurement times are equal and always cover one modulation period with 100 time steps. (The error is plotted versus the light center frequency f_c and the relative variation $I_{s,\Delta}$ of the scattered light. Error values outside the range are shown in white.)

tion), $M = 1$ modulation cycle and $N = 100$ time steps are considered. The resulting systematic errors $\Delta(v)$ are shown in Fig. 7 with respect to f_c and $I_{s,\Delta}$ for the different DGV approaches. As expected, 1-ν-DGV is not affected by scattered light fluctuations and therefore the error is zero. Regarding DGV approaches with laser frequency modulation, FM-DGV shows the lowest errors over a wide parameter range. This is due to the

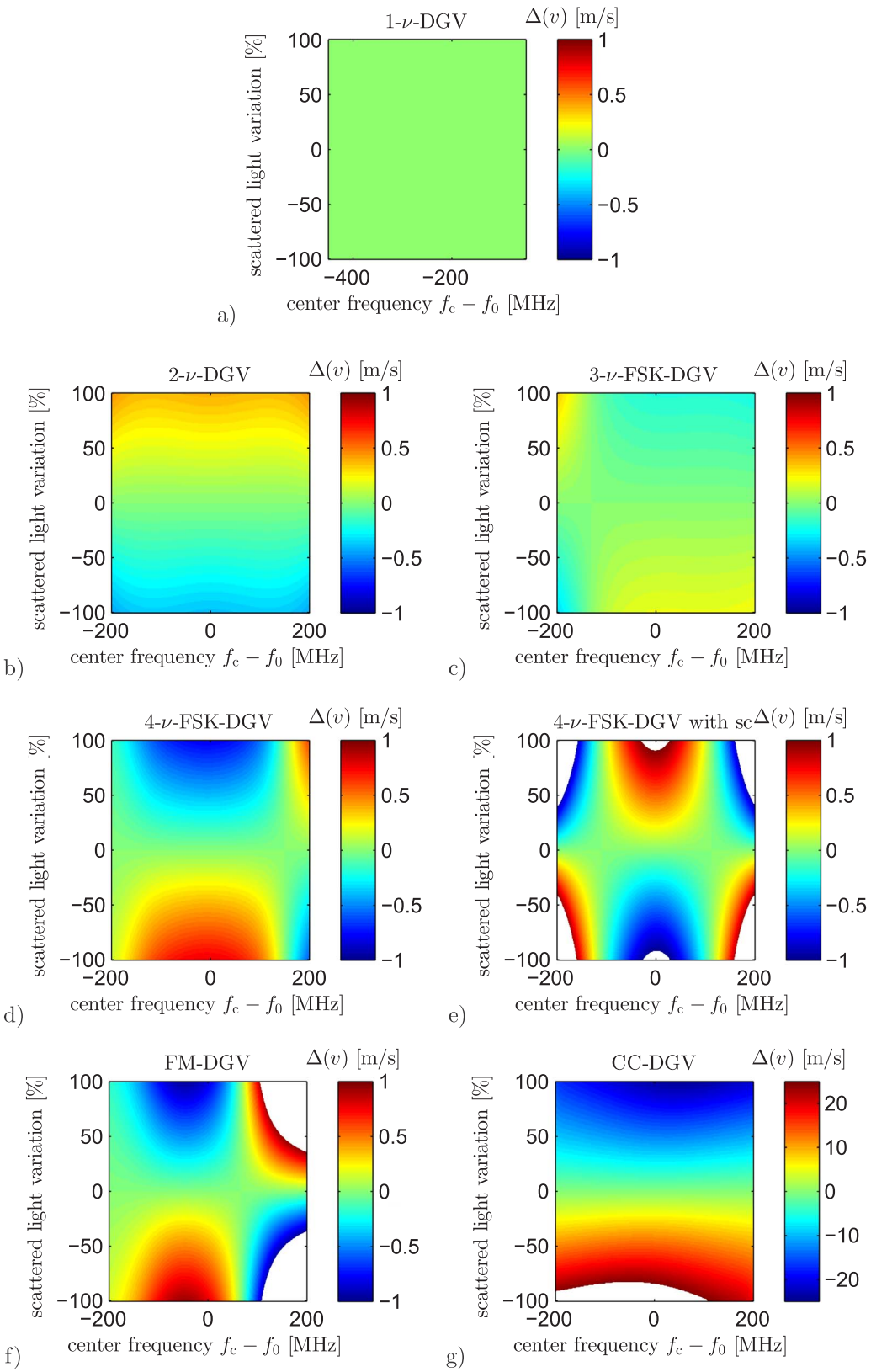

Fig. 8. Systematic velocity error for the different DGV approaches under *camera-limited condition* resulting from a linear variation of the scattered light power. The measurement times are equal, but the modulation periods are different. (The error is plotted versus the light center frequency f_c and the relative variation $I_{s,\Delta}$ of the scattered light. Error values outside the range are shown in white.)

high number of time steps (here: $N = 100$), which is larger than the minimal number of required time steps and therefore allows (at least partially) a correction of the scattered light fluctuations using the proposed signal processing algorithm, see Section 2. Note that the same phenomenon is already visible when comparing 4-ν-FSK-DGV with 3-ν-FSK-DGV. The fourth additional time step allows a partial correction of

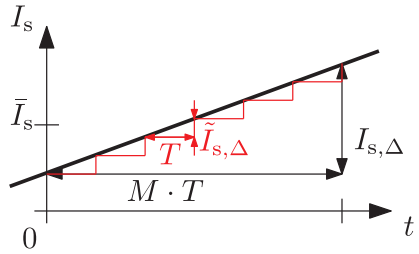

Fig. 9. Scattered light intensity I_s versus time and the observed fluctuation $I_{s,\Delta}$ of the scattered light intensity. One measurement over the measurement time $M{\cdot}T$ can be considered as a series of M subsequent sub-measurements, where M is the number of modulation cycles (here: $M=6$) during the measurement time and T is the duration of one modulation cycle. By decreasing T, the observed variation $\tilde{I}_{s,\Delta}$ of the scattered light intensity during one modulation cycle (one sub-measurement) is reduced.

the scattered light variation. It is remarkable that, even for the maximal linear increase of the scattered light, the absolute value of the error is below 5 m/s for FM-DGV. In principle, CC-DGV has the same potential as FM-DGV, but its current signal processing algorithm offers no such correction. For this reason, the performance of CC-DGV is here similar to the remaining DGV approaches. In summary, the absolute value of the error is, e.g., well below 20 m/s for $|I_{s,\Delta}| \leq 50\%$ in the considered measurement range. Although the error can attain larger values than the uncertainty limit discussed in Section 3, it depends on the flow velocity if it is a significant error source and if the error is acceptable or not. With respect to fast flows with velocities of several hundred meters per second such as occurring in turbomachinery or high-pressure fuel injections, the maximal error is surprisingly low.

The second case of different modulation periods (camera-limited condition) means that the number of modulation cycles during the constant measurement time can be increased. Since each modulation cycle allows one velocity measurement, it is then possible to average over multiple velocity measurements with a shorter temporal resolution. However, the increase of the number of measurements is limited by the maximal frame rate of the camera and the number of time steps per modulation cycle. Considering 100 time steps, the respective maximal number of modulation cycles reads $M = 100/N$ with N as the number of time steps per modulation cycle. For FM-DGV and CC-DGV, $N=10$ and $N=100$ is chosen, respectively. For the other DGV approaches see Table 2. The resulting velocity errors with respect to f_c and $I_{s,\Delta}$ are shown in Fig. 8 for the different DGV approaches. No error occurs for 1-ν-DGV, and the error is within $\pm$ 0.4 m/s for 2-ν-DGV and 3-ν-FSK-DGV. The largest errors occur for CC-DGV. Comparing with the laser-limited condition, cf. Fig. 7, the resulting errors have not changed for 1-ν-DGV and CC-DGV, because the measurement conditions are the same. Note, however, that the error for CC-DGV would decrease when the number of time steps is increased or when the required number of time steps per modulation cycle is decreased, respectively. For all other DGV variants, the resulting error for under camera-limited condition is shown to be smaller than for the laser-limited condition, because the modulation periods are decreased or the number of modulation cycles during the constant measurement time is increased, respectively.

As a general trend of the systematic errors due to fluctuations of the scattered light power, the error magnitude is related directly to the number of time steps per modulation cycle or indirectly to the number of modulation cycles, respectively. The reason is as follows: Since each modulation cycle allows to perform one sub-measurement, decreasing the time steps per modulation cycle means averaging over an increasing number of sub-measurements while the temporal resolution of these sub-measurements becomes higher. Due to the increased temporal resolution, the observed variation of the scattered light during the sub-measurement becomes smaller and, thus, the error is reduced, cf. Fig. 9. Hence, the error is minimal for DGV techniques that require a minimal number of time steps per modulation cycle. The initial concern regarding the DGV approaches with laser frequency modulation is in principle correct. However, the concrete measurement task finally decides, if this error can be tolerated or not and if other aspects are more important.

5. Fluctuations of the velocity

The simulations from Section 4 are repeated, but now with a constant scattered light intensity and a linear temporal variation of the flow velocity:

$$v_i = \bar{v}\cdot\left(1 + v_\Delta\cdot\left(\frac{i}{N\cdot M} - \frac{1}{2}\right)\right),$$
$$i = 0,\ 1,\ \ldots,\ N\cdot M - 1. \tag{24}$$

The mean velocity is $\bar{v}$ and the total change of velocity is v_Δ. The investigated range of v_Δ is from -100 m/s to $+100$ m/s. According to the proportionality between velocity and Doppler frequency of 1.58 MHz/(m/s), cf. Section 2, the range of the corresponding Doppler frequency variations amounts to $\pm$ 158 MHz. All other parameters are the same as in Section 5.

The comparison of the DGV approaches for an equal modulation period, i.e., for the laser-limited condition, is presented in Fig. 10 ($M=1$ modulation cycles, $N=100$ time steps). The calculated systematic deviations $\Delta(v)$ from the mean velocity are shown over f_c and v_Δ. As an important result, all DGV variants are influenced by velocity variations. The lowest error occurs for 1-ν-DGV and FM-DGV. Within $|v_\Delta| < 50$ m/s for instance, the absolute value of the error is below 5 m/s. Actually, 1-ν-DGV performs a direct averaging of the different velocity values as along as the used region of the transmission curve is linear. FM-DGV benefits again from the high number of available time steps and the signal processing in the frequency domain, which obviously allow a reduction of the resulting error. Within $|v_\Delta| < 50$ m/s, the other DGV variants perform qualitatively different but quantitatively similar with a maximum error in the order of 10 m/s. This illustrates the importance of minimizing the modulation period, so that the flow velocity variation during the modulation cycle becomes negligibly small or the resulting error becomes tolerable.

The DGV comparison for different modulation periods (and an equal measurement time), i.e., for the camera-limited condition, is presented in Fig. 11. Except for CC-DGV, the absolute value of the error of all DGV approaches is well below 5 m/s for $|v_\Delta| < 50$ m/s, while the differences are considered to be marginal. Comparing with the laser-limited condition, cf. Fig. 10, the resulting errors remain unchanged for 1-ν-DGV and CC-DGV, because the measurement conditions are the same again. Note that the unchanged error for CC-DGV is due to the chosen boundary condition, where the number of time steps equals the given number of required time steps per modulation cycle for CC-DGV. The error for CC-DGV would decrease when the number of time steps is increased or when the required number of time steps per modulation cycle is decreased, respectively. For all other DGV variants, the error is shown to be smaller for camera-limited condition than for laser-limited condition, because the number of modulation cycles is increased, which means more sub-measurements during the constant measurement time. The effect is the same as for the scattered light fluctuations discussed in Section 4.

In conclusion, DGV techniques with and without laser frequency modulation are considered to have similar capabilities regarding flows with fast varying flow velocities.

6. Conclusions and outlook

An overview of the existing DGV measurement approaches with and without laser frequency modulation was presented. All methods can be categorized by the required number of time steps. While all approaches attain equal spatial resolutions, the temporal resolution decreases with an increasing number of time steps, when being limited by the maximal

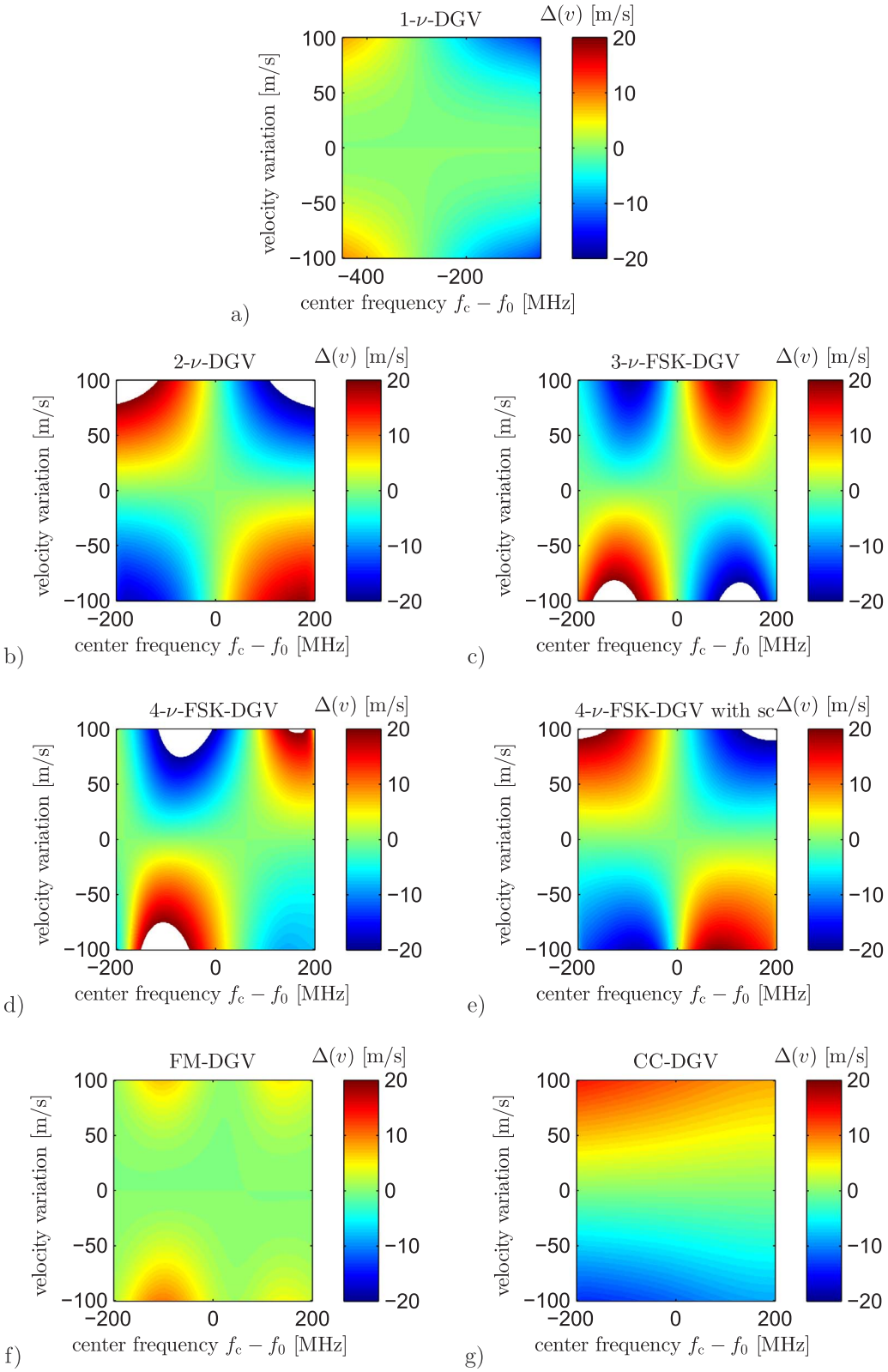

Fig. 10. Systematic velocity error for the different DGV approaches under *laser-limited condition* resulting from a linear variation of the velocity. The measurement times are equal and always cover one modulation period with 100 time steps. (The error is plotted versus the light center frequency f_c and the velocity variation v_Δ. Error values outside the range are shown in white.)

camera frame. However, with an increasing number of time steps, the measurements include self-corrections of possible errors, e.g., due to background light changes and transmission curve changes. The available measurement ranges are similar except for the CC-DGV, which provides in principle an unlimited measurement range. Hence, CC-DGV is appropriate for flows with hundreds to thousands of meters per second.

The comparison of the calculated Cramér-Rao bound with respect to

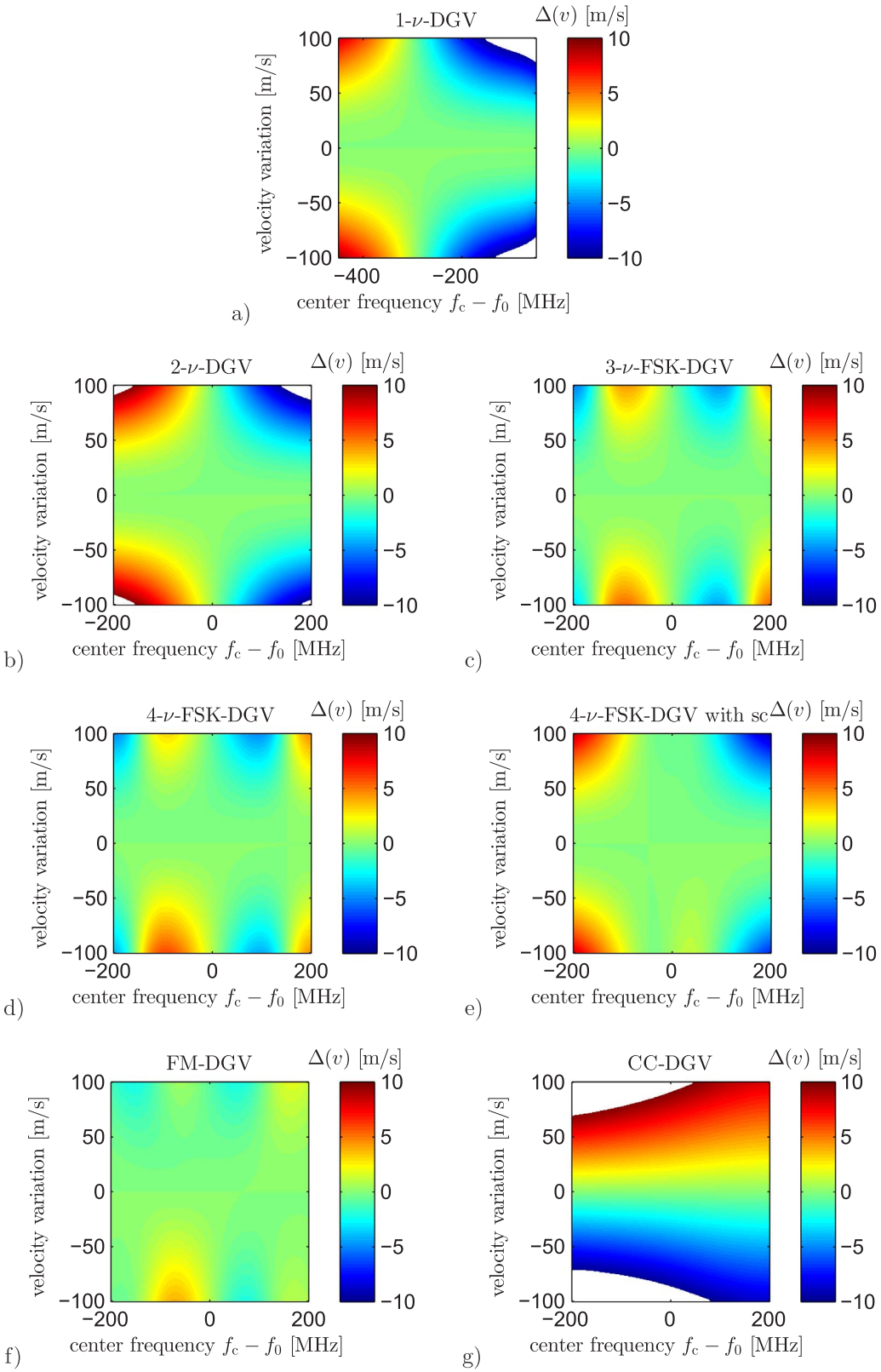

Fig. 11. Systematic velocity error for the different DGV approaches under *camera-limited condition* resulting from a linear variation of the velocity. The measurement times are equal, but the modulation periods are different. (The error is plotted versus the light center frequency f_c and the velocity variation v_Δ. Error values outside the range are shown in white.)

photon shot noise identified no superior technique, because the respective fundamental limits of the measurement uncertainty are close to each other. A simpled relation was derived, which allows to calculate the fundamental limit of the DGV measurement uncertainty as a function of the available number of scattered photons. While CC-DGV has the lowest signal processing efficiency, which can be improved in future for instance by optimizing the number of correlation data points that are used for the parabolic fit or by changing the model function for the fit, the signal processing of all other DGV techniques is well-developed, because the variances of the estimators attain or almost attain the Cramér-Rao bound. Systematic deviations did not occur, although the signal processings usually contain a division and, thus, a non-linearity. It is assumed that the investigated signal-to-noise ratio was high enough so that the effect of the non-linearity becomes negligible. However, future studies should investigate the possible bias of the signal processings for measurements at a low signal-to-noise-ratio.

DGV without laser frequency modulation is sensitive with respect to spatial fluctuations of the scattered light intensity, whereas DGV with laser frequency modulation is sensitive with respect to temporal fluctuations of the scattered light intensity. Simulations revealed the quantitative errors resulting from temporal intensity fluctuations of the scattered light. For equal modulation periods and an equal measurement time, the smallest errors are obtained with FM-DGV and (after revising the signal processing) CC-DGV. These are the DGV techniques with the largest number of time steps and therefore the signals contain the most information. For different modulation periods but still an equal measurement time, which applies when being limited by the frame rate of the camera, the smallest errors are obtained with the fewest number of time steps per modulation cycle using 2-ν-DGV and 3-ν-FSK-DGV. Of course, no such error occurs for 1-ν-DGV with one time step. However, the experimental conditions and the measurement task finally decide whether a DGV system without or with laser frequency modulation is appropriate. For instance, for ultra-high-speed investigations with measurement rates in the MHz range, which are desired for understanding the dynamical behavior of high-pressure fuel injections, DGV without laser frequency modulation is the fastest option. For combustion measurements, the systematic error of the background light from the flame are inherently eliminated when using FM-DGV as an example. In addition, while DGV without laser frequency modulation usually requires two cameras and image dewarping techniques to eliminate the errors due to spatial fluctuations of the scattered light intensity, DGV with laser frequency modulation are single-camera techniques and have no such cross-sensitivity.

All DGV approaches suffer from variations of the flow velocity during the measurement. For the case of equal modulation periods, 1-ν-DGV and FM-DGV show the lowest resulting error. For the case of different modulation periods and an equal measurement time, all DGV variants perform similar except for CC-DGV, where the largest errors occur. As a common result for DGV without and with laser frequency modulation, the velocity variation is identified as one possibly critical error source when investigating fast varying flow.

In conclusion, a model-based review of all DGV measurement techniques was presented. Furthermore, the fundamental limit of the measurement uncertainty due to photon shot noise was calculated and the systematic errors due to variations of the scattered light intensity and the flow velocity were described. Note that many further error sources such as multiple scattering, reflexes from walls, laser stability, stability of the transmission curve and detector noise have not been considered here, because these errors are suspected to be similar for the various DGV methods [84,66]. However, future studies of the DGV measurement uncertainty can enhance the model-based review of the different DGV measurement techniques by incorporating these effects.

References

[1] Adrian RJ. Particle-imaging techniques for experimental fluid mechanics. Annu Rev Fluid Mech 1991;23:261–304.
[2] Wernet MP. Two-dimensional particle displacement tracking in particle imaging velocimetry. Appl Opt 1991;30(14):1839–46.
[3] Maas HG, Gruen A, Papantoniou D. Particle tracking velocimetry in three-dimensional flows – part 1: photogrammetric determination of particle coordinates. Exp Fluids 1993;15(2):133–46.
[4] Malik NA, Dracos T, Papantoniou DA. Particle tracking velocimetry in three-dimensional flows – part II: particle tracking. Exp Fluids 1993;15(4):279–94.
[5] Cierpka C, Kähler C.J. Cross-correlation or tracking – comparison and discussion. In: Proceedings of the 16th international symposium on applications of laser techniques to fluid mechanics. Lisbon, number 2.1.3; 2012. p. 10.
[6] Westerweel J. Fundamentals of digital particle image velocimetry. Meas Sci Technol 1997;8(12):1379–92.
[7] Adrian RJ. Twenty years of particle image velocimetry. Exp Fluids 2005;39(2):159–69.
[8] Wernet MP. Temporally resolved PIV for space-time correlations in both cold and hot jet flows. Meas Sci Technol 2007;18(5):1387–403.
[9] Hain R, Kähler CJ. Fundamentals of multiframe particle image velocimetry (PIV). Exp Fluids 2007;42(4):575–87.
[10] Cenedese A, Cenedese C, Furia F, Marchetti M, Moroni M, Shindler L. 3D particle reconstruction using light field imaging. In: Proceedings of the 16th international symposium on applications of laser techniques to fluid mechanics. Lisbon, number 1.1.2; 2012. p. 9.
[11] Thompson DH. A tracer-particle fluid velocity meter incorporating a laser. J Phys E: Sci Instrum 1968;1(9):929–32.
[12] Tanner LH. A particle timing laser velocity meter. Opt Laser Technol 1973;5(3):108–10.
[13] Schodl R. A laser-two-focus (L2F) velocimeter for automatic flow vector measurements in the rotating components of turbomachines. J Fluids Eng 1980;102(4):412–9.
[14] Aizu Y, Asakura T. Principles and development of spatial filtering velocimetry. Appl Phys B: Lasers Opt 1987;43(4):209–24.
[15] Aizu Y, Asakura T. Spatial filtering velocimetry: fundamentals and applications. Berlin: Springer; 2005.
[16] Hosokawa S, Mastumoto T, Tomiyama A. Tomographic spatial filter velocimetry for three-dimensional measurement of fluid velocity. In: Proceedings of the 16th international symposium on applications of laser techniques to fluid mechanics. Lisbon, number 1.9.2; 2012. p. 12.
[17] Yeh Y, Cummins HZ. Localized fluid flow measurements with an He-Ne laser spectrometer. Appl Phys Lett 1964;4(10):176–8.
[18] Albrecht H-E, Borys M, Damaschke N, Tropea C. Laser Doppler and phase Doppler measurement techniques. Berlin: Springer; 2003.
[19] Coupland J. Coherent detection in Doppler global velocimetry: a simplified method to measure subsonic fluid flow fields. Appl Opt 2000;39(10):1505–10.
[20] Meier AH, Rösgen T. Heterodyne Doppler global velocimetry. Exp Fluids 2009;47(4):665–72.
[21] Meier AH, Rösgen T. Imaging laser Doppler velocimetry. Exp Fluids 2012;52(4):1017–26.
[22] Tropea C. Laser Doppler anemometry: recent developments and future challenges. Meas Sci Technol 1995;6(6):605–19.
[23] Büttner L, Czarske J. A multimode-fibre laser-Doppler anemometer for highly spatially resolved velocity measurements using low-coherence light. Meas Sci Technol 2001;12(11):1891–903.
[24] Czarske J. Laser Doppler velocity profile sensor using a chromatic coding. Meas Sci Technol 2001;12(1):52–7.
[25] Czarske Jürgen, Büttner Lars, Razik Thorsten, Müller Harald. Boundary layer velocity measurements by a laser Doppler profile sensor with micrometre spatial resolution. Meas Sci Technol 2002;13(12):1979–89.
[26] Voigt A, Bayer C, Shirai K, Büttner L, Czarske J. Laser Doppler field sensor for high resolution flow velocity imaging without camera. Appl Opt 2008;47(27):5028–40.
[27] Smeets G, George A. Michelson spectrometer for instantaneous Doppler velocity measurements. J Phys E: Sci Instrum 1981;14(7):838–45.
[28] Seiler F, Oertel H. Visualization of velocity fields with Doppler-pictures. In: Proceedings of the 3rd international symposium on flow visualization. Ann Arbor (Michigan); 1983.
[29] Seiler F, George A, Srulijes J, Havermann M. Progress in Doppler picture velocimetry (DPV). Exp Fluids 2008;44(3):389–95.
[30] Landolt A, Roesgen T. Anomalous dispersion in atomic line filters applied for spatial frequency detection. Appl Opt 2009;48(31):5948–55.
[31] Landolt A, Rösgen T. Global Doppler frequency shift detection with near-resonant interferometry. Exp Fluids 2009;47(4–5):733–43.
[32] Lu Z-H, Charett TOH, Ford HD, Tatam RP. Mach-Zehnder interferometric filter based planar Doppler velocimetry (MZI-PDV). J Opt A: Pure Appl Opt 2007;9(11):1002–13.
[33] Lu Z-H, Charett TOH, Tatam RP. Three-component planar velocity measurements using Mach-Zehnder interferometric filter-based planar Doppler velocimetry (MZI-PDV). Meas Sci Technol 20(3):034019; 2009. p. 15.
[34] Jackson DA, Paul DM. Measurement of hypersonic velocities and turbulence by direct spectral analysis of Doppler shifted laser light. Phys Lett 1970;32A(2):77–8.

[35] Seasholtz RG, Buggele AE, Reeder MF. Flow measurements based on Rayleigh scattering and Fabry-Perot interferometer. Opt Laser Eng 1997;27(6):543–70.
[36] Kentischer TJ, Schmidt W, Sigwarth M, Uexküll Mv. TESOS, a double Fabry-Perot instrument for solar spectroscopy. Astron Astrophys 1998;340:569–78.
[37] Chehura E, Ye C-C, Tatam RP. In-line laser Doppler velocimeter using fibre-optic Bragg grating interferometric filters. Meas Sci Technol 2003;14(6):724–35.
[38] Komine H. System for measuring velocity field of fluid flow utilizing a laser-Doppler spectral image converter. US Patent 4 919 536; 1990.
[39] Meyers JF, Komine H. Doppler global velocimetry – a new way to look at velocity. In: Proceedings of the 4th international conference on laser anemometry – advances and applications. Cleveland (Ohio); 1991. pp. 289–96.
[40] Meyers JF. Development of Doppler global velocimetry as a flow diagnostic tool. Meas Sci Technol 1995;6(6):769–83.
[41] Arnette SA, Samimy M, Elliot GS. Two-component planar Doppler velocimetry in the compressible turbulent boundary layer. Exp Fluids 1998;24(4):323–32.
[42] Röhle I, Willert CE. Extension of Doppler global velocimetry to periodic flows. Meas Sci Technol 2001;12(4):420–31.
[43] Willert C, Stockhausen G, Beversdorff M, Klinner J, Lempereur C, Barricau P, et al. Application of Doppler global velocimetry in cryogenic wind tunnels. Exp Fluids 2005;39(2):420–30.
[44] Willert C, Stockhausen G, Klinner J, Lempereur C, Barricau P, Loiret P, et al. Performance and accuracy investigations of two Doppler global velocimetry systems applied in parallel. Meas Sci Technol 2007;18(8):2504–12.
[45] Morrison GL, Gaharan CA. Uncertainty estimates in DGV systems due to pixel location and velocity gradients. Meas Sci Technol 2001;12(4):369–77.
[46] Ainsworth RW, Thorpe SJ, Manners RJ. A new approach to flow-field measurement – a view of Doppler global velocimetry techniques. Int J Heat Fluid Flow 1997;18(1):116–30.
[47] Arnette SA, Elliott GS, Mosedale AD, Carter CD. A two-color approach to planar Doppler velocimetry. In: AIAA Proceedings of the 36th aerospace sciences meeting. Reno (Nevada), number AIAA-98-0507; 1998. p. 20.
[48] Arnette SA, Carter CD. Two-color planar doppler velocimetry. AIAA J 2000;38(11):2001–6.
[49] Charrett TOH, Ford HD, Nobes DS, Tatam RP. Two-frequency planar Doppler velocimetry (2-ν-PDV). Rev Sci Instrum 2004;75(11):4487–96.
[50] Charrett TOH, Tatam RP. Single camera three component planar velocity measurements using two-frequency planar Doppler velocimetry (2ν-PDV). Meas Sci Technol 2006;17(5):1194–206.
[51] Müller H, Eggert M, Pape N, Dopheide D, Czarske J, Büttner L, Razik T. Time resolved DGV based on laser frequency modulation. In: Proceedings of the 12th international symposium on applications of laser techniques to fluid mechanics. Lisbon, number 25.2; 2004. p. 10.
[52] Müller H, Eggert M, Czarske J, Büttner L, Fischer A. Single-camera Doppler global velocimetry based on frequency modulation techniques. Exp Fluids 2007;43(2):223–32.
[53] Eggert M, Müller H, Czarske J, Büttner L, Fischer A. Self-calibrating single camera Doppler global velocimetry based on frequency shift keying. In: Nitsche W, Dobriloff C, editors, Imaging measurement methods for flow analysis. Springer, Berlin; 2009. pp. 43–52.
[54] Fischer A, Büttner L, Czarske J, Eggert M, Grosche G, Müller H. Investigation of time-resolved single detector Doppler global velocimetry using sinusoidal laser frequency modulation. Meas Sci Technol 2007;18(11):2529–45.
[55] Fischer A, Büttner L, Czarske J, Eggert M, Müller H. Array Doppler global velocimeter with laser frequency modulation for turbulent flow analysis – sensor investigation and application. In: Nitsche W, Dobriloff C, editors, Imaging measurement methods for flow analysis. Springer, Berlin; 2009. pp. 31–41.
[56] Cadel DR, Lowe KT. Cross-correlation Doppler global velocimetry (CC-DGV). Opt Lasers Eng 2015;71:51–61.
[57] Cadel DR, Lowe KT. Investigation of measurement sensitivities in cross-correlation Doppler global velocimetry. Opt Lasers Eng 2016;86:44–52.
[58] Fischer A, König J, Czarske J, Rakenius C, Schmid G, Schiffer H-P. Investigation of the tip leakage flow at turbine rotor blades with squealer. Exp Fluids 54(2):1462; 2013. p. 15.
[59] Haufe D, Schlüßler R, Fischer A, Büttner L, Czarske J. Optical multi-point measurement of the acoustic particle velocity in a superposed flow using a spectroscopic laser technique. Meas Sci Technol 23(8):085306; 2012, p. 8.
[60] Fischer A, König J, Haufe D, Schlüßler R, Büttner L, Czarske J. Optical multi-point measurements of the acoustic particle velocity with frequency modulated Doppler global velocimetry. J Acoust Soc Am 2013;134(2):1102–11.
[61] Haufe D, Fischer A, Czarske J, Schulz A, Bake F, Enghardt L. Multi-scale high-speed measurement of acoustic particle velocity and flow velocity for liner investigations. Exp Fluids 54(7):1569; 2013. p. 7.
[62] Haufe D, Schulz A, Bake F, Enghardt L, Czarske J, Fischer A. Spectral analysis of the flow sound interaction at a bias flow liner. Appl Acoust 2014;81:47–9.
[63] Schlüßler R, Bermuske M, Czarske J, Fischer A. Simultaneous three-component velocity measurements in a swirl-stabilized flame. Exp Fluids 56(10):183; 2015. p. 13.
[64] Herring GC, Meyers JF, Hart RC. Shock-strength determination with seeded and seedless laser methods. Meas Sci Technol 20(4):045304; 2009. p. 9.
[65] Meyers JF, Lee JW, Cavone AA. Boundary layer measurements in a supersonic wind tunnel using Doppler global velocimetry. In: Proceedings of the 15th international symposium on applications of laser techniques to fluid mechanics. Lisbon, number 1.8.1; 2010, p. 11.
[66] Fischer A, Haufe D, Büttner L, Czarske J. Scattering effects at near-wall flow measurements using Doppler global velocimetry. Appl Opt 2011;50(21):4068–82.
[67] Schlüßler R, Blechschmidt C, Czarske J, Fischer A. Optimizations for optical velocity measurements in narrow gaps. Opt Eng 52(9):094101; 2013. p. 9.
[68] Fischer A, Büttner L, Czarske J, Eggert M, Müller H. Measurements of velocity spectra using time-resolving Doppler global velocimetry with laser frequency modulation and a detector array. Exp Fluids 2009;47(4):599–611.
[69] Willert C, Hassa C, Stockhausen G, Jarius M, Voges M, Klinner J. Combined PIV and DGV applied to a pressurized gas turbine combustion facility. Meas Sci Technol 2006;17(7):1670–9.
[70] Fischer A, König J, Czarske J, Peterleithner J, Woisetschläger J, Leitgeb T. Analysis of flow and density oscillations in a swirl-stabilized flame employing highly resolving optical measurement techniques. Exp Fluids 54(2):1622; 2013. p. 18.
[71] Röhle I. Three-dimensional Doppler global velocimetry in the flow of a fuel spray nozzle and in the wake region of a car. Flow Meas Instrum 1996;7(3–7):287–94.
[72] Thorpe SJ, Quinlan N, Ainsworth RW. The characterisation and application of a pulsed neodymium YAG laser DGV system to a time-varying high-speed flow. Opt Laser Technol 2000;32(7–8):543–55.
[73] Fischer A, Schlüßler R, Haufe D, Czarske J. Lock-in spectroscopy employing a high-speed camera and a micro-scanner for volumetric investigations of unsteady flows. Opt Lett 2014;39(17):5082–5.
[74] Fischer A, Wilke U, Schlüßler R, Haufe D, Sandner T, Czarske J. Extension of frequency modulated Doppler global velocimetry for the investigation of unsteady spray flows. Opt Lasers Eng 2014;63:1–10.
[75] Schlüßler R, Gürtler J, Czarske J, Fischer A. Planar near-nozzle velocity measurements during a single high-pressure fuel injection. Exp Fluids 56:176; 2015. p. 11.
[76] Fischer A, König J, Czarske J. Speckle noise influence on measuring turbulence spectra using time-resolved Doppler global velocimetry with laser frequency modulation. Meas Sci Technol 19(12):125402; 2008. p. 15.
[77] Schlüßler R, Czarske J, Fischer A. Uncertainty of flow velocity measurements due to refractive index fluctuations. Opt Lasers Eng 2014;54:93–104.
[78] Chan VSS, Heyest AL, Robinson DI, Turner JT. Iodine absorption filters for Doppler global velocimetry. Meas Sci Technol 1995;6(6):784–94.
[79] Fischer A, Büttner L, Czarske J. Simultaneous measurements of multiple flow velocity components using frequency modulated lasers and a single molecular absorption cell. Opt Commun 2011;284(12):3060–4.
[80] Steck DA. Cesium D Line Data (rev. 2.1.1). University of Oregon, Department of Physics, available online at ⟨http://steck.us/alkalidata⟩ (revision 2.1.4); 2010.
[81] Fischer A, Büttner L, Czarske J, Eggert M, Müller H. Measurement uncertainty and temporal resolution of Doppler global velocimetry using laser frequency modulation. Appl Opt 2008;47(21):3941–53.
[82] Forkey JN, Lempert WR, Miles RB. Corrected and calibrated I_2 absorption model at frequency-doubled Nd:YAG laser wavelengths. Appl Opt 1997;36(27):6729–38.
[83] McKenzie RL. Measurement capabilities of planar Doppler velocimetry using pulsed lasers. Appl Opt 1996;35(6):948–64.
[84] Fischer A, Pfister T, Czarske J. Derivation and comparison of fundamental uncertainty limits for laser-two-focus velocimetry, laser Doppler anemometry and Doppler global velocimetry. Measurement 2010;43(10):1556–74.